Functionalized nanoporous gold as a new biosensor platform for ultra-low quantitative detection of human serum albumin

Elsevier Editorial System(tm) for Sensors & Actuators: B. Chemical

Manuscript Draft

Manuscript Number: SNB-D-18-05491R2

Title: Functionalized Nanoporous Gold as a new Biosensor Platform for Ultra-low Quantitative Detection of Human Serum Albumin

Article Type: Research Paper

Keywords: De-alloying; nanoporous gold; functionalization; Human Serum Albumin; selective binding; Surface Enhanced Raman Spectroscopy

Corresponding Author: Professor Paola Rizzi, Ph.D.

Corresponding Author's Institution: Università di Torino

First Author: Federico Scaglione, PhD

Order of Authors: Federico Scaglione, PhD; Eugenio Alladio, PhD; Alessandro Damin, PhD; Francesco Turci, PhD; Claudio Baggiani, prof; Cristina Giovannoli, prof; Silvia Bordiga, prof; Livio Battezzati, prof; Paola Rizzi, Ph.D.

Abstract: The development of a new generation of ultra-sensitive sensors for analytical and bio-diagnostic devices requires a strong signal in front of very small quantity of analyte, often present in complex and interfering matrix. Taking advantage of peculiar plasmonic properties of nanoporous gold (NPG), a promising sensor for selective detection of Human Serum Albumin (HSA), a proof-of-concept bioanalyte, was prepared and tested in a conventional micro-Raman spectrometer using Surface Enhanced Raman Spectroscopy (SERS). NPG was synthesized by chemical de-alloying of an amorphous precursor, $Au_{20}Cu_{48}Ag_7Pd_5Si_{20}$, starting from melt spun ribbons. A fully de-alloyed ribbon with ligaments of about 60 nm was obtained after 4 h of de-alloying at 70° C and 10 M HNO_3 + 0.5 M HF. This material is self-standing, mechanically resistant, and suitable for wide range of applications. At this stage, NPG is SERS-active toward several molecules, including pyridine, bi-pyridine, and rhodamine at very low concentration. In order to obtain the selective binding properties required to detect molecules in bio-diagnostic applications, immuno-functionalization of NPG was carried out by using an anti-HSA antibody (Ab-anti-HSA) covalently grafted on gold ligaments via the 4-aminothiophenol (4ATP) Raman probe, yielding the SERS-active nanohybrid NPG-4ATP-Ab. SERS signal recorded at increasing HSA concentrations was used for the acquisition of SERS maps and a chemometric regression model allowed to calibrate the sensor. In the best experimental conditions, we were able to get quantitative analysis of HSA at ultra-low concentrations (0.1 ng/l) with SERS.
The methodology proposed in this paper has to be considered a major step toward a calibrated device for ultra-sensitive detection of biomolecules by SERS detection.

Research Data Related to this Submission

There are no linked research data sets for this submission. The following reason is given:

Data will be made available on request

***Response to Reviewers**

Manuscript reference number: SNB-D-18-05491

Title: Functionalized Nanoporous Gold as a new Biosensor Platform for Ultra-low Quantitative Detection of Human Serum Albumin

Dear Editor,

the suggested correction addressed by Reviewer # 1 (i.e. to change the word “field intensity” with “field amplitude”) was addressed in the corrected version of the manuscript.

Your faithfully

Paola Rizzi

Functionalized Nanoporous Gold as a new Biosensor Platform for Ultra-low Quantitative Detection of Human Serum Albumin

F. Scaglione, E. Alladio, A. Damin, F. Turci, C. Baggiani, C. Giovannoli,

S. Bordiga, L. Battezzati, P. Rizzi

Dipartimento di Chimica and NIS, Università di Torino, V. Giuria 7, 10125 Torino, Italy.

E-mail address of authors:

federico.scaglione@unito.it

eugenio.alladio@unito.it

alessandro.damin@unito.it

francesco.turci@unito.it

claudio.baggiani@unito.it

cristina.giovannoli@unito.it

silvia.bordiga@unito.it

livio.battezzati@unito.it

paola.rizzi@unito.it (Corresponding author)

Abstract

The development of a new generation of ultra-sensitive sensors for analytical and bio-diagnostic devices requires a strong signal in front of very small quantity of analyte, often present in complex and interfering matrix. Taking advantage of peculiar plasmonic properties of nanoporous gold (NPG), a promising sensor for selective detection of Human Serum Albumin (HSA), a proof-of-concept bioanalyte, was prepared and tested in a conventional micro-Raman spectrometer using Surface Enhanced Raman Spectroscopy (SERS). NPG was synthesized by chemical de-alloying of an amorphous precursor, $Au_{20}Cu_{48}Ag_7Pd_5Si_{20}$, starting from melt spun ribbons. A fully de-alloyed ribbon with ligaments of about 60 nm was obtained after 4 h of de-alloying at 70° C and 10 M HNO_3 + 0.5 M HF. This material is self-standing, mechanically resistant, and suitable for wide range of applications. At this stage, NPG is SERS-active toward several molecules, including pyridine, bi-pyridine, and rhodamine at very low concentration. In order to obtain the selective binding properties required to detect molecules in bio-diagnostic applications, immuno-functionalization of NPG was carried out by using an anti-HSA antibody (Ab-anti-HSA) covalently grafted on gold ligaments via

the 4-aminothiophenol (4ATP) Raman probe, yielding the SERS-active nanohybrid NPG-4ATP-Ab. SERS signal recorded at increasing HSA concentrations was used for the acquisition of SERS maps and a chemometric regression model allowed to calibrate the sensor. In the best experimental conditions, we were able to get quantitative analysis of HSA at ultra-low concentrations (0.1 ng/l) with SERS.

The methodology proposed in this paper has to be considered a major step toward a calibrated device for ultra-sensitive detection of biomolecules by SERS detection.

Keywords: De-alloying; nanoporous gold; functionalization; Human Serum Albumin; selective binding; Surface Enhanced Raman Spectroscopy.

1. Introduction

Diagnostic tools based on sensitive and selective sensors are expected to foster the development of cutting-edge key-enabling technologies (KETs). As future innovation drivers, KETs are crucial to help applied research to stay at the front line of innovation [1]. Specifically, accessible and affordable devices for the detection of pathogenic agents, disease markers, food safety, and environmental contaminants strongly relies on the availability of sensors that combine analytic specificity with high signal-to-noise ratio [2]. The development of a new generation of ultra-sensitive sensors, requiring very small quantities of molecules for giving a strong response, is expected to boost a variety of applications ranging from point-of-care tests [3], wearable devices and self bio-diagnostic [4,5,6].

In this context, Surface Enhanced Raman Spectroscopy (SERS) is a very sensitive and versatile technique of investigation in the field of both fundamental and applied research, as resulting from the rich scientific and patent literature [7,8]. In fact, the single-molecule sensitivity that can be nominally reached by this technique makes SERS a potential candidate for the development of advanced, innovative, and affordable sensors based on vibrational spectroscopy.

SERS takes advantage of the enhancement of Raman signal observed when molecules interact with a nano-structured metallic materials, typically chemically inert precious metals. Nanostructured precious metals often possess peculiar plasmonic features, which result in a strong absorption of electro-magnetic radiations. The wavelength at which the absorption is maximized and, consequently, the enhancement of Raman signal is observed, is strongly connected to the dimension and the shape of the metallic nano-

structure. Therefore, SERS effect can be maximized by controlling carefully the morphological features of metallic nanostructures. For biosensing applications, different SERS-active surfaces substrata can be discriminated according to the enhancement factor (EF) which may affect the limit of detection (LOD) of a given analyte [9]. EF, that is proportional to the fourth power of the field amplitude interacting with the probe molecule, is due to chemical and electromagnetic effects. Basically, the chemical effect is caused by the charge transfer between the adsorbed molecules and the nano-structured metallic substrate and has a very limited contribution (two orders of magnitude lower) to the overall EF value [10,11], whereas the electromagnetic effect arising from the resonant excitation of localized surface plasmons in the proximity of the metallic surface can dramatically increase the EF [12]. The electromagnetic field enhancement is strongly related to specific features on the nano-structure, i.e. interparticle gaps [13], sharp edges [14], and nanopores [15, 16], typically referred as ‘‘hot spots”. For these reasons, the development of an innovative SERS-active surface goes necessarily through the optimization of the metallic nano-structured materials

Nanoporous gold (NPG) is a 3D-scaffold material constituted by nano-sized pores and ligaments. Strategies for efficient NPG synthesis involve the anodic roughening of Au films [17, 18] or de-alloying of Au alloys. In particular, binary systems (e.g. Cu-Au [19], Ag-Au [20, 21]) or complex Au-based amorphous alloys [22, 23, 24, 25] are currently the best candidates to NPG preparation via de-alloying. Being a versatile, rapid, and simple route for NPG preparation, de-alloying procedure allows to tune finely gold micro- and nano-structure by tailoring the composition of the starting alloy and the etching conditions, namely electrolyte composition, temperature, potential, and time of treatment. De-alloying of amorphous Au-alloys allows to create morphologically different NPG on order to maximize the plasmonic effects [26,27].

Currently, de-alloying of Au-based amorphous precursors are achieved by electrochemical or chemical procedures giving rise to nanoporous Gold, with ligament size ranging from 40 to 200 nm [28,29]. Morphology can be tailored by changing de-alloying conditions such as electrolyte, temperature and time, giving rise to materials with characteristic properties. Due to a peculiar nano-grained structures of ligaments, NPGs obtained from amorphous precursors were demonstrated to be more active when compared with Nanoporous Gold produced starting from crystalline precursors. Applications of nanoporous Gold were successfully reported as electrodes for the electro-oxidation of methanol [30], electro-catalysts for the hydrogen evolution reaction [31] and SERS substrate with high plasmonic properties [32,33]. Moreover, NPG does not requires supports (i.e. it is a free-standing material), is mechanically stable, it can be bent and

manipulated without breaking, a crucial point for substrates that need to be handle several time for applications.

In this work, a new ultra-sensitive SERS sensor for analytical and bio-diagnostic devices was prepared by de-alloying an amorphous melt spun ribbon precursor ($Au_{20}Cu_{48}Ag_7Pd_5Si_{20}$). Human Serum Albumin (HSA) was chosen as a proof of concept analyte and NPG was imunofunctionalized with an anti-HSA rabbit antibody (Ab anti-HSA) covalently grafted on gold ligaments via the 4-aminothiophenol (4ATP), a Raman probe already described, yielding the SERS-active nanohybrid NPG-4ATP-Ab (f-NPG). SERS mapping of f-NPG interacting with increasing concentrations of HSA was carried out on a conventional micro-Raman spectrometer. Calibration of the sensor was performed by regression and predictive discriminant analysis taking advantage of a chemometric approach suitable to analyse the modification of the entire spectrum instead of the local changes in minor features of specific Raman peaks.

This work aims to prepare a reproducible and ultra-sensitive sensor able to detect quantitatively a wide range of bioanalytes at ultra-low concentrations. SERS on nanostructured f-NPG allows fast and sensitive analytical response.

The device proposed has been studied to be selective for HSA by adopting a proper functionalization. The use of HSA was adopted as a proof of concept to show the potentiality of the device. The methodology and results, reported in the following, suggest this device would be able to detect other appealing antigen once provided a proper antibody functionalized at the device surface.

2. Material and Methods

2.1 Materials

4-aminothiophenol (4ATP), 4-mercaptobenzoic acid (4MBA), cysteamine (CYS), 3-mercaptopropionic acid (3MPA), acid 2-(N-morpholino) ethanesulfonic acid (MES), 1-ethyl-3-(3-dimethylaminopropyl) carbodiimide (EDC), N,N'-diisopropylcarbodiimide (DIC), N-hydroxysuccinimide (NHS), dimethylformamide (DMF), anti-HSA antibody (pAb) produced in rabbit, Bovine Serum Albumin (BSA), Human Serum Albumin (HSA), Tween 20 surfactant were purchased from Sigma (Milan, Italy). All the electrolyte and buffered solutions were prepared with chemical grade reagents dissolved in ultrapure water obtained from Purelab Prima System, Elga (Bucks, UK).

2.2. Preparation of nanoporous gold (NPG)

A master alloy ingot of composition $Au_{20}Si_{20}Cu_{48}Ag_7Pd_5$ (at.%) was prepared by arc-melting lamps of pure elements (Au: 99.99%, Si: 99.9995%, Ag, Cu, Pd: 99.99%) in Ti-gettered Argon atmosphere, to avoid oxidation. Master alloy ingot was then rapidly quenched by melt-spinning technique; during rapid solidification, the melt contained in a quartz crucible was spun onto a copper wheel rotating at a speed rate of 20-25 m/s. The heat of the molten alloy was rapidly dispersed by the wheel and solidification occurs in form of ribbons, avoiding crystallization. Ribbons were 20-25 μm thick, 2 mm wide and appeared to be fully amorphous at an X-ray Diffraction (XRD) analysis.

De-alloying of ribbons was performed by chemical means in a mixture of 10 M HNO_3 + 0.5 M HF at 70 °C for 4 hours; etching conditions were carefully set to obtain the desired NPG. The addition of HF was designed to avoid the formation of SiO_2 when the Silicon contained in the alloy precursor is oxidized [28].

After de-alloying, NPG samples were rinsed with ultrapure water to remove the excess of acid solution inside pores and then air-dried. The microstructure and structure of de-alloyed samples were studied by Scanning Electron Microscopy (SEM) with Energy Dispersive X-ray Spectroscopy (EDS) after Co calibration and X-ray Diffraction (XRD) in Bragg-Brentano geometry with Cu-K_α radiation. Ligaments size was measured at their narrower necks using a Leica software [29].

2.3. Preparation of SERS-active surfaces

Nanoporous gold strips two centimetres long were put into glass vials used as reactors. Glassware and NPG strips were preliminary washed with a Piranha acid solution (sulfuric acid:hydrogen peroxide, 7+3 v/v) and rinsed with plenty of ultrapure water until neutral pH. 1 mL of a 1% w/v ATP ethanolic solution was dispensed into the vials and left to react overnight at 4°C (**Fig. 1a**). NPG strips were rinsed with ethanol and air-dried. The same procedure was also performed with the other thiol-based compounds considered in this study like 4-mercaptobenzoic acid, cysteamine and 3-mercaptopropionic acid in order to obtain surfaces with different SERS reports (CYS-NPG, 3MPA-NPG, 4MBA-NPG).

Covalent immobilization of anti-HSA Ab on 4ATP-NPG (**Fig. 1b**) was performed by NHS/ECD activation method widely described in literature [34]. Breafly, 2 mL of a 0.4 mM EDC + 0.1 mM NHS solution were mixed with 2 mL of a 1:5000 diluted anti-HSA Ab solution - both freshly prepared in 50 mM MES buffer at pH 5.5 - and left to react 2 hours at 4°C. Afterwards, 1 mL of the activated solution was

dispensed into the vial containing 4ATP-NPG. The mixture was allowed to react overnight at 4°C. To wash away the unconjugated antibody three consecutive washing steps were performed by adding a 0.05 % v/v Tween 20 aqueous solution to the vial and removing it by aspiration. The blocking step was performed by incubating 1 mL of 1 mg/mL BSA solution in phosphate buffer (20 mM pH 7.4, 0.13 M NaCl, PBS) for 1 hour at 4°C (**Fig. 1c**). Proven that BSA does not interfere at all, this step allowed the blockage of any remaining active site on the gold surface preventing non-specific interactions. Lastly, functionalised nanoporous gold strips were washed three times with a 0.05 % v/v Tween 20 aqueous solution to get the final SERS-active surface named hereafter as f-NPG. At this stage, f-NPG was ready for reaction with the specific analyte (HSA) and subsequent SERS mapping.

With regard to f-NPG functionalised with SERS reporter provided with carboxylic group (i.e. 4MBA) the covalent immobilisation of Ab anti-HSA was performed by a two-step conjugation. Briefly, 1 mL of a 0.5 mM DIC + 0.5 mM NHS dimethylformamide solution was dispensed into the vial containing 4MBA-NPG and left to react 1 hour at room temperature. After its removing, 1 mL of a 1:10000 diluted anti-HSA Ab carbonate buffer solution (50 mM pH 9.0) was dispensed into the vial and left to react 1 hour at room temperature. To wash away the unconjugated antibody three consecutive washing steps were performed by adding a 0.05 % v/v Tween 20 aqueous solution to the vial and removing it by aspiration.

The cleaning procedure in Piranha was moreover used to restore NPG samples after functionalization and SERS measurements up to twenty times. Piranha solution does not affect the surface of NPG neither in the size of ligaments nor in the chemical composition. Since the SERS behaviour is strictly related to morphology and composition of the substrate, plasmonic properties of the restored ad re-functionalized samples are maintained after each cleaning step.

2.4 Colorimetric detection of NPG functionalization.

A colorimetric detection based on the reaction with a HRP-labelled goat anti-rabbit antibody (Sigma, Milan, Italy) able to bind anti-HSA antibody (raised in rabbit) covalently immobilized on NPG surface was performed. Briefly, 1 mL of a 1:3000 diluted HRP-labelled goat anti-rabbit antibody solution in phosphate buffer (0.5 % w/v BSA added) was dispensed into the vial and left to react for an hour at 37°C. After removing the unbound labelled antibody by washing with a 0.05 % v/v Tween 20 aqueous solution, 1 mL of 3,3′,5,5′-tetramethylbenzidine/H_2O_2 solution (ready-to-use, Sigma) was added. After 10 minute the reaction

was stopped by addition of a sulphuric acidic solution, then the absorbance was read at 450 nm.

2.5. SERS measurements.

Measurements were performed with a Renishaw inVia Raman Microscope, equipped with multi-wavelength lasers ranging from UV to NIR, using 785 nm laser line with an acquisition time of 20 s, 10% (4 mW) power at the surface and a 5x objective. Maps of 100 points were collected on functionalized NPG (f-NPG) after each incubation step in HSA at increasing concentrations. The spectrometer was calibrated before measurements using the Raman band of silicon wafer at 520 cm^{-1}.

Nanoporous Gold samples were incubated in HSA solution and then measured by acquiring 100 points SERS maps after drying. This procedure was repeated starting from a low concentration of 0.1 ng/L up to 100 μg/L. A map at 0 ng/L (i.e. f-NPG before incubation with any HSA solution) has been collected to appreciate shift variations and intensity of ν(SC) peak at increasing HSA concentrations. Maps have been acquired physically on the same grid of points thanks to an optimized sample-holder able to fix the sensor during the incubation step and using the coordinates of the Raman micro-camera to find a specific position.

2.6.Computational details.

Calculations were performed by adopting the Gaussian09 [35] code (release D.01) and an Au_{13} cluster, as a model of Au surface and as proposed in literature [36]. The hybrid functional B3LYP [37,38] coupled to the empirical dispersive term, as proposed in the D2 Grimme scheme [39] (hereafter referred as B3LYP-D2) were employed through the whole set of calculations. Default parameters for the integration scheme were chosen. All electron standard Pople Gaussian basis sets were used for describing respectively H/C/N/O (6-31+G(2d,p)) and S (6-31+G(2df,p)) species. For Au atoms a standard LanL2DZ pseudo-potential was adopted, coupled to the corresponding LanL2DZ basis set for describing the remaining electrons (19 on total of 79). Bare Au_{13} cluster was fully optimized (2S+1=2) without symmetry constraints. For calculations (2S+1=1) regarding the adsorption of molecular species of interest, positions of Au atoms were kept fixed at those of the optimized bare Au_{13} cluster, and just H/C/N/O/S atoms was allowed to relax. The same holds for the case where Au_4 cluster (obtained by cutting a portion of Au_{13}) is present.

2.7 Binding studies

HSA dilutions in PBS buffer with the addition of 0.05% v/v Tween 20, and 0.5 % w/v BSA were prepared in the range from 0.1 ng/L to 100 μg/L (0.1, 1, 2, 3, 5, 6, 10, 20, 30, 60, 100 ng/L, 0.2, 0.3, 0.6, 1, 2, 3, 6, 10, 20, 30, 60, 100 μg/L). The additions of Tween 20 and BSA were made in order to prevent protein to protein interactions and non specific protein adsorption to f-NPG surface.

The reading of the zero SERS signal corresponding to zero HSA concentration was performed by direct contact of f-NPG with the diluent buffer. Starting from the lower HSA concentration, 100 μL was dispensed on f-NPG surface, left to incubate for 1 hour at room temperature and then rinsed with 0.05 % v/v Tween 20 aqueous solution to remove the unbound protein. f-NPG was then dried under a gentle stream of nitrogen. At this stage, f-NPG is ready for SERS detection (**Fig. 1d**).

2.8. Partial least squares regression (PLS) model.

Pre-processing approaches of median centering, automatic Weighted Least Squares (WLS) baseline and Savitzky-Golay smoothing was employed on the measured data before calculating the PLS model. Log-10 scaled concentrations were used, too, for all the tested samples. Genetic algorithms were performed for features selection purposes and performance parameters such as PRESS, RMSEC, RMSECV and R^2 were evaluated.

3. Results and Discussion

The selection of NPG for this work results from a series of different nanoporous Au ribbons prepared in recent years. Exploring the $Au_{40-x}Cu_{28+x}Ag_7Pd_5Si_{20}$ (with x= 0, 10, 20) compositions, different amorphous ribbons have been prepared and NPGs with ligament dimensions ranging from ~40 to ~200 nm have been obtained by chemical or electrochemical de-alloying, changing etching parameters. All NPGs have shown SERS activity with probe molecules [15, 40]. In particular, the NPG prepared from $Au_{20}Cu_{48}Ag_7Pd_5Si_{20}$, used in this work as self-standing, shows superior SERS activity achieving a detection limit down to 10^{-14} M using 4,4-bi-pyridine and 10^{-6} M with melamine in aqueous solution as probe molecule. For this material, the enhancement factor of NPG was calculated with respect to standard Raman on flat gold and was estimated to be around 2×10^{13} [41]. This value is much higher than that of NPG de-alloyed from crystalline alloys (around 10^6) and of wrinkled nanoporous gold (around 10^8), making this substrate an ideal candidate for SERS applications [27,42]. Its high plasmonic activity and low values of LOD have been attributed to

different aspects: i) a fine nano-sized ligaments structure enhancing the localized electromagnetic fields, ii) the electromagnetic coupling between ligaments and iii) the presence of trapped SERS sensitive elements such as Ag and Pd.

3.1 Characterization of the Nanoporous Gold substrate

De-alloying of $Au_{20}Cu_{28}Ag_7Pd_5Si_{20}$ ribbons by chemical means in a mixture of 10 M HNO_3 + 0.5 M HF at 70 °C for 4 hours has led to a NPG constituted by a fine microstructure composed by pores and ligaments (**Fig. 2a).** The selective dissolution of the amorphous precursor has occurred from the external surface inside the whole thickness of the strip (**Fig. 2b)**; while the less noble elements of the matrix have been dissolved in the electrolyte as ions, adatoms of Au have reorganized along the solid/electrolyte interfaces by surface diffusion into interconnected ligaments separated by porosities [43]. Ligaments have an average size of 60 nm measured at their narrower necks and are constituted by several randomly oriented nano-crystals impinged each other forming grain boundaries and other crystallographic defects that enable the formation of rough ligament surfaces (**Fig. 2b inset**). This morphology is peculiar when de-alloying occurs in an amorphous structure where a long range atomic order is not present and Au adatoms do not have a crystalline lattice to adapt to, during surface diffusion, for building up crystalline ligaments. In this case, rather differently compared with de-alloying of crystalline solid solutions [44,45], the nucleation and growth of nanocrystals occurs to form ligaments, replacing the amorphous structure [46,47]. During de-alloying, as a consequence of the surface diffusion driving mechanism, less noble atoms (i.e. Ag, Pd) might be incorporated as impurity in the newly formed crystals and ligaments; their presence within the fine and defective morphology of ligaments has been proved increasing the catalytic properties [30] and the plasmonic effect of the substrate [15].

3.2 Functionalization of Nanoporous Gold substrate

In order to study the Raman signal produced by modified NPG substrates, four different compounds (i.e. cysteamine, 3-mercaptopropionic acid, 4-aminothiophenol, 4-mercaptobenzoic acid) all provided with a sulfidrilic group to be bound to the gold surface, were tested after their immobilization on nano-structured gold surface of given porosity (**Fig. S1**, Supporting info). The structural differences among the selected molecules concern the functional group (i.e. amino or carboxyl) used to link covalently the antibody and the

aliphatic or aromatic nature of the structure themselves. All these molecules are bifunctional with a thiol group able to form the Au-S bond to NPG and an amino or carboxylic terminal group that gives an amide bond with the antibody. Aromatic moieties have been preferred to aliphatic ones due to a more oriented interaction of the molecule with the NPG surface, while the choice between the two aromatic moieties (i.e. 4ATP and 4MBA) has been affected by the strategy used to generate the amide bond with the antibody.

To investigate the differences of f-NPG binding properties obtained by adopting two functionalization methods (i.e. the activation of antibody carboxylic groups through a fully aqueous approach and the activation of SERS reporter carboxylic groups in DMF as described in §2.3), we performed a colorimetric detection based on the use of a goat HRP-labelled anti-rabbit antibody able to bind the anti-HSA antibody covalently immobilized on the surface **(Fig 3a)**. The binding curves obtained **(Fig. 3b)** show higher absorbance values when the antibody immobilization is performed by NHS/EDC method and using 4ATP as SERS reporter respect to what observed with 4MBA. Primarily, these results do confirm that both methods have been able to functionalize NPG surfaces. Besides, the fully aqueous approach, proved to be more friendly for the exclusion of organic solvents, appears to give a more functionalized NPG surface. Therefore, the approach using 4ATP molecule as SERS reporter has been chosen to carry on our study, being the more efficient.

The whole functionalization occurs in steps as described in detail in §2.3 [48].

3.3 Optimization of SERS signal

A preliminary study of the SERS parameters influencing the Raman signal was performed, in order to optimize the measurement conditions. The size of the beam spot (i.e. magnification of the lens) defines the area where the signal is collected. Our findings prove that the use of a beam spot giving information on an extended area, decreases the variability of readings due to the random distribution of hot spots, typical of SERS measurements [14]. For this reason a 5x objective has been selected, with a spot area of 20 μm x 2 μm.

Once set the spot size, the power at the surface and the acquisition time (i.e. time of interaction of the beam with the surface) have been optimized. Low power means few counts at the detector and a disadvantageous signal-to-noise ratio, while increasing too much the power might burn the organic functionalization of f-NPG in the worst case, or simply giving decomposition or dimerization of ATP at the

surface [49]. The best compromise has been found selecting an acquisition time of 20 s and 10% (4 mW) power at the surface. In these operating conditions the signal has an high signal-to-noise ratio and the heat generated by the laser does not affect the f-NPG surface.

In **Fig. 3c** it is reported a typical SERS spectrum experimentally obtained from f-NPG measurements together with the full assignment of SERS signals. Regardless of the interaction with HSA, the signals are associated to specific vibrational modes of the adsorbed 4-ATP and in good agreement with values found in the literature [50, 51, 52, 53, 54]. Among several peaks associated to vibrational modes of the aromatic rings of the molecule, the most intense signal at 1081 cm^{-1} has been attributed to the stretching of ν(SC). This peak within other parameters have been considered for the analyses of SERS spectra as a function of HSA concentration.

3.4 Sensor characterization

Once prepared f-NPG according to the previously described functionalization, f-NPG has been incubated in solutions at increasing HSA concentration and then measured by acquiring 100 points SERS maps after drying. This procedure has been repeated starting from a low concentration of 0.1 ng/L up to 100 μg/L.

According to experimental conditions described in §2.5 a complete SERS mapping of f-NPG has been recorded in the entire range of concentration considered.

As can be observed from SERS maps reported in **Fig. 4a,b,c,d,e,** the intensity of ν(SC) peak increases increasing the amount of HSA bound selectively on the sensor. This trend is observed in all grid positions even where more active points (i.e. hot spots) are present. The change of the average value of the intensity is shown in **Fig. 4f**: grid points have been divided in three groups with low, medium and high SERS activity and the average intensity within the standard error has been plotted vs HSA concentration.

Furthermore, the ν(SC) peak position at several HSA dosages is analysed in SERS maps (**Fig. 4g,h** and **Fig. S2** supporting information). It can be clearly observed how ν(SC) peak moves towards higher Raman shifts (blue-shift, $\Delta\nu(SC)>0$). This perturbative effect is more evident at low HSA concentration (**Fig. 7a**, 0.1 ng/l peak) and it decreases for increasing concentration (**Fig. 7a**, 1 ng/l peak) to reach a mean value (**Fig. 7a** from 10 ng/l to 60000 ng/l peaks) due to cooperative phenomena acting on the functionalized surface.

In order to get some insights for the comprehension of such behaviour, quantum-mechanics based calculations of Raman spectra (see Computational details for an extended description of the adopted

methodology) have been performed on simplified models of the sensor. **Fig. 5** is reporting a graphical representation of two possible models for f-NPG.

The simplest one (hereafter f-NPG-I, see **Fig. 5a**) is constituted by an Au_{13} cluster simulating the surface of NPG, and by a grafted 4-mercaptoaniline emisuccinamide molecule (SC_6H_4-NHCO-C_2H_4-COOH) simulating the pab-ATP receptor for HSA. In order to take into account for possible lateral interaction between the receptor and other portions of the extended NPG surface, a more complex model (hereafter f-NPG-II) has been developed by adding a supplementary Au_4 cluster at a fixed distance from Au_{13} (**Fig. 5c**). Finally, the HSA adsorption at f-NPG has been modelled through the interaction between f-NPG-I/II and formic acid (HCOOH) used as a target, as schematized in **Fig. 5b,d,e**.

Raman spectra computed on f-NPG-I prior and after the interaction with HCOOH are reported in **Fig. 6a** (red and blue solid lines respectively): in this case just a small perturbation of ν(SC), and with the wrong sign (red-shift or $\Delta\nu(SC)<0$, being $\Delta\nu(SC) = \nu(SC)^{\text{f-NPG-I/II}} - \nu(SC)^{(\text{f-NPG-I/II})\cdots\text{HCOOH}}$), is visible as a consequence of the interaction of f-NPG-I (the simplified model for f-NPG) with the target molecule (*i.e.* HCOOH, the simplified model for HSA), so being quite far from the experimental observation.

As far as f-NPG-II model is concerned, Raman spectra computed on the naked model and after its interaction with HCOOH are reported in **Fig. 6b**: in this case two possible situations concerning the interaction of f-NPG-II with HCOOH have been analyzed. In one case the target molecule (HCOOH) resulted to be able to interact with both the receptor (grafted on Au_{13}) and the Au_4 cluster: Raman spectrum computed for this situation (see blue solid line in **Fig. 6b**) shows a consistent red-shift of ν(SC) ($\Delta\nu(SC)<0$) when compared to its position in the Raman spectrum computed for the bare f-NPG-II (red solid line in **Fig. 6b**). Conversely, when HCOOH is supposed to specifically interact with the receptor (grafted on Au_{13}), so that the last one is moved far away from the original position in bare f-NPG-II (where the end of the chain is interacting with Au_4 too), ν(SC) underwent an appreciable blue-shift ($\Delta\nu(SC)>0$, see green solid line in **Fig. 6b**), as proved by the experimental observations. It is worth mentioning that, even if models used are over simplified with respect to the real system, it is evident that Raman bands are sensible to the environment in a consistent way.

3.5 Sensor calibration and data treatment

In order to obtain quantitative information from SERS maps, a calibration of the sensor is needed and the

chemometric approach is necessary to build a model fitting experimental data.

In particular, Partial Least Squares (PLS) [55] regression approach was employed to build a reliable model on the available data. The predictive ability of the PLS was evaluated on the 100-points SERS maps collected at different HSA concentration levels, i.e. from of 0.1 ng/L up to 100 μg/L. In details, the following concentrations (ng/L), for an overall amount of 29 independent samples, were evaluated: 0, 0.1 (2 samples), 1 (2 samples), 2, 3, 5, 6, 10 (2 samples), 20, 30, 60, 100 (2 samples) ng/L, 2, 3, 6, 10, 20, 30, 60, 100 μg/L).

The map collected at 0 ng/L (i.e. f-NPG before interaction with any HSA solutions) was considered as a blank reference sample, whose signals were subtracted to the measured SERS maps at different concentration levels after performing the data pre-treatment process.

SERS maps reported in Figure 4 shows that the blank sample (0 ng/l) has an average intensity that is higher than the those of 0.1 and 1 ng/l, respectively. However, as it can be seen in the new Figure S3, that is reported within the supplementary information, the blank sample shows a higher baseline than 0.1 and 1 ng/l samples. Furthermore, before calculating the PLS-GA model, it is necessary to uniform the data by using specific data pre-processing strategies. In particular, the following pre-processing techniques were employed before computing the PLS regression model: median centering, automatic Weighted Least Squares (WLS) baseline algorithm and Savitzky-Golay smoothing approaches [56, 57]. The application of median centering, automatic Weighted Least Squares (WLS) and Savitzky-Golay's smoothing firstly allow to perceive that the intensity of the main ν(SC) peak increases as a function of HSA concentration. Secondly, it can be observed that the blank sample has slightly lower intensities than the 0.1 ng/l spectrum at the main ν(SC) peak. For this reason, the blank sample was subtracted from all the SERS spectra. Figure S3 shows this concept by focusing on the concentrations equal to 0, 0.1, 1, 5 and 10 ng/l, but the same results are observed with all the other concentrations, as it can also be seen in Figure 7.

The pre-processing algorithms were performed with the help of MATLAB software version R2018b with PLS_Toolbox version 8.7. **Fig. 7a** reports the SERS spectra after the pre-processing techniques, showing the increasing intensity of the ν(SC) peak as a function of HSA concentration and a blue-shift more evident for low concentration values that tend to reach a mean value with lower blue-shift for increasing HSA concentrations as described before.

More in details, a polynomial of order 3 and number of 15 points in the Savitzky-Golay filter was selected, together with the order of 0 for the derivative function. A **X** matrix of dimensions 28 × 575 was

then arranged consisting of the measured 28 samples (0 ng/L blank sample was excluded) and 575 wavelengths (ranging from 806 up to 1349 cm^{-1}), respectively. Moreover, a **Y** matrix of dimensions 28 × 1 was arranged too, containing the increasing concentration levels of the measured samples, transformed into log-10 scale. A cross-validation (CV) procedure was performed when building the PLS model by applying a venetian blinds design on a number of data splits equal to 5. The whole data set was randomly divided into different training and evaluation sets consisting of 22 and 6 samples, respectively, for numerous times. The number of latent variables (LV) was selected according to the predictive residual error sum of square (PRESS), multiple correlation coefficient (R^2) and root mean square error in cross-validation (RMSECV) [56]. Further parameters were monitored too, such as Q residuals, Hotelling T^2, leverages and Y-studentized residuals [58, 59]. Additionally, genetic algorithms (GA) approach [60, 61, 62] of features selection was applied to the preliminary PLS model, aiming to optimize it, by selecting the most relevant wavelengths for regression purpose. GA approach was tested several times to validate our approach by evaluating the most robust PLS model, i.e. the ones providing the lowest values of root mean square error in calibration (RMSEC) and cross-validation (RMSECV). Moreover, prediction uncertainty was estimated by evaluating the standard error of calibration (SEC) and some metrics remarked by Zhang and Garcia-Munoz [63]. The developed PLS model is shown in **Fig. 7b**, where the *x-axis* represents the prepared and measured HSA concentrations (ng/L, log-10 scale), while the *y-axis* shows the HSA concentration levels estimated by our model (ng/L, log-10 scale). 7 LVs were selected and quite low results of RMSEC and RMSECV were achieved (i.e. being respectively equal to 0.217 and 0.557), together with remarkable values of R^2 (i.e. 0.984 and 0.891 for calibration and cross-validation models, respectively) and an acceptable overall uncertainty of ±7.5%. In particular, PLS-GA approach provided this robust model for the prediction of HSA concentrations by selecting the predictors within the wavelengths' ranges of 992-1021 cm^{-1}, 1072-1096 cm^{-1}, 1132-1153 cm^{-1}, and 1167-1192 cm^{-1}.

Fig. 7b provides also a proof of the reproducibility of measurements using restored and re-functionalized NPG substrates. Double points at the same abscissa value mean two maps acquired physically on two different NPG pieces: overlapped circles demonstrate not only the homogeneity in terms of morphology among different pieces of substrate but also in terms of reproducible SERS response.

3.6 Application of the PLS method

The PLS-GA regression model is itself a calibration of the HSA sensor and it can be used to have a quantitative prediction on an unknown HSA concentration interacting with the functionalized sensor.

Being a proof-of-concept, the use of PLS on SERS maps, in combination with GA, provided robust predictions of HSA, within a wide range of log-10 scaled concentrations. Improved results might be achieved in the future by monitoring lower and selected ranges of concentrations. The LOD value reported in this study is used to show the advantages of the PLS approach when used as a calibration model. In the present case, LOD is represented as a proof-of-concept of the fact that the interpretation of SERS maps via a combination of pre-processing techniques and PLS-GA approach might allow to reach very low concentration in a significant and robust way. However, further samples and evaluations have to be performed to calculate LOD and, eventually, LOQ (limit of quantitation) values in a proper way.

4. Conclusions

A NPG prepared by free corrosion of an amorphous precursor was fully de-alloyed by chemical mean and then functionalized with specific antibody selective for Human Serum Albumin. The functionalized substrate (f-NPG) was tested by acquiring SERS maps at increasing concentration of the analyte. Maps showed an increase of the intensity as a function of HSA concentration and a blue shift of the Raman signal, more evident for low concentration values. Quantum-mechanic calculations of Raman spectra suggested that the blue shift of the main signal might be due to lateral interactions of the receptor with NPG.

Data analyses in junction with a PLS-GA chemometric approach successfully demonstrated that the proposed sensor is able to detect HSA at ultra-low concentration, from a proof-of-concept LOD value of 0.1 ng/L up to 0.1 mg/l.

The methodology proposed in this paper is a major step toward a calibrated device for ultra-sensitive detection of biomolecules with SERS.

Acknowledgments

This work was supported by Convenzione Compagnia di San Paolo, BINGO Project–Torino_call2014_L2_146. Acquisition of the SEM images has been performed thanks to NanoFacility Piemonte, INRIM.

References

1. Chapman, C. A. R., *et al.*, *Advanced Functional Materials* (2017) **27** (3), 1604631
2. Jaramillo, D. X. O., *et al.*, *Electroanalysis* (2017) **29** (10), 2316
3. Garcia-Gradilla, V., *et al.*, *Small* (2014) **10** (20), 4154
4. Sriwichai, S., *et al.*, *Journal of Applied Polymer Science* (2018) **135** (1), 45641
5. Ju, H., *Applied Materials Today* (2018) **10**, 51
6. Lin, Z.-H., *et al.*, *Chemical Communications* (2011) **47** (25), 7116
7. Xue, L., *et al.*, *Small* (2017) **13** (22), 1603947
8. Sharma, B., *et al.*, *Materials Today* (2012) **15** (1-2), 16
9. Qin, Z., *et al.*, *Journal of Physics D: Applied Physics* (2008) **41** (15), 152007
10. Schatz, G. C., and Van Duyne, R. P., *Hand Book of Vibrational Spectroscopy* (2002), 759
11. Morton, S. M., and Jensen, L., *Journal of the American Chemical Society* (2009) **131** (11), 4090
12. Pieczonka, N. P. W., and Aroca, R. F., *Chemical Society Reviews* (2008) **37** (5), 946
13. Lim, D.-K., *et al.*, *Nature Nanotechnology* (2011) **6**, 452
14. Zhang, L., *et al.*, *RSC Advances* (2016) **6** (4), 2882
15. Scaglione, F., *et al.*, *Philosophical Magazine Letters* (2015) **95** (9), 474
16. Zhang, X., *et al.*, *Advanced Materials* (2015) **27** (6), 1090
17. Xu, S. L., *et al.*, *Int. J. Electrochem. Sci.* (2013) **8** (2), 1863
18. Fang, C., *et al.*, *RSC Adv.* (2014) **4** (37), 19502
19. Morrish, R., *et al.*, *Scripta Materialia* (2011) **64** (9), 856
20. Lu, X., *et al.*, *Scripta Materialia* (2007) **56** (7), 557
21. Erlebacher, J., *et al.*, *Nature* (2001) **410**, 450
22. Scaglione, F., *et al.*, *Intermetallics* (2010) **18** (12), 2338
23. Yu, J., *et al.*, *Chemistry of Materials* (2008) **20** (14), 4548
24. Abe, H., *et al.*, *Materials Transactions* (2009) **50** (6), 1255
25. Battezzati, L., and Scaglione, F., *Journal of Alloys and Compounds* (2011) **509**, S8
26. Lang, X., *et al.*, *Applied Physics Letters* (2011) **98** (9), 093701
27. Zhang, L., *et al.*, *ACS Nano* (2011) **5** (6), 4407
28. Xue, Y., *et al.*, *Corrosion Science* (2017) **127**, 141
29. Scaglione, F., *et al.*, *Journal of Alloys and Compounds* (2014) **615**, S142
30. Paschalidou, E. M., *et al.*, *Journal of Alloys and Compounds* (2016) **667**, 302
31. Scaglione, F., *et al.*, *Journal of Materials Science* (2018) **53** (17), 12388
32. Xue, Y., *et al.*, *Applied Surface Science* (2019) **476**, 412
33. Xue, Y., *et al.*, *Chemical Physics Letters* (2018) **709**, 46
34. Sehgal, D., and Vijay, I. K., *Analytical Biochemistry* (1994) **218** (1), 87
35. Frisch, M. J., *et al.*, Gaussian 16 Rev. B.01. Wallingford, CT, (2016)
36. Zhao, L.-B., *et al.*, *The Journal of Chemical Physics* (2011) **135** (13), 134707
37. Becke, A. D., *The Journal of Chemical Physics* (1993) **98** (2), 1372
38. Lee, C., *et al.*, *Physical Review B* (1988) **37** (2), 785
39. Grimme, S., *Journal of Computational Chemistry* (2006) **27** (15), 1787
40. Xue, Y., *et al.*, *Chemical Physics Letters* (2016) **665**, 6
41. Xue, Y., *et al.*, *Applied Surface Science* (2017) **426**, 1113
42. Liu, H., *et al.*, *Scientific Reports* (2011) **1** (1)
43. Paschalidou, E. M., *et al.*, *Acta Materialia* (2016) **119**, 177
44. Scaglione, F., *et al.*, *Intermetallics* (2015) **66**, 82
45. Petegem, S. V., *et al.*, *Nano Letters* (2009) **9** (3), 1158
46. Rizzi, P., *et al.*, *Journal of Alloys and Compounds* (2014) **586**, S117
47. Scaglione, F., *et al.*, *Journal of Alloys and Compounds* (2012) **536**, S60
48. Srivastava, S. K., *et al.*, *Small* (2014) **10** (17), 3579
49. Fang, Y., *et al.*, *Langmuir* (2010) **26** (11), 7737
50. Abdelsalam, M., *Open Chemistry* (2009) **7** (3)
51. Kim, K., and Yoon, J. K., *The Journal of Physical Chemistry B* (2005) **109** (44), 20731
52. Varsanyi, G., *Vibrational Spectra of Benzene Derivatives*. 1969
53. Uetsuki, K., *et al.*, *J. Phys. Chem. C* (2010) **114** (16), 7515
54. Gabudean, A. M., *et al.*, *Journal of Molecular Structure* (2011) **993** (1), 420
55. Wold, S., *et al.*, *Chemometrics and Intelligent Laboratory Systems* (2001) **58** (2), 109
56. Rinnan, Å., *et al.*, *TrAC Trends in Analytical Chemistry* (2009) **28** (10), 1201
57. Savitzky, A., and Golay, M. J. E., *Analytical Chemistry* (1964) **36** (8), 1627
58. Geladi, P., and Kowalski, B. R., *Analytica Chimica Acta* (1986) **185**, 1
59. Slutsky, B., *Journal of Chemical Information and Computer Sciences* (1998) **38** (6), 1254
60. Leardi, R., and Gonzalez, A. L., *Chemometrics and Intelligent Laboratory Systems* (1998) **41** (2), 195
61. Leardi, R., *Journal of Chemometrics* (2000) **14** (5-6), 643

62. Alladio, E., *et al.*, *Anal Chim Acta* (2015) **878**, 78
63. Zhang, L., and Garcia-Munoz, S., *Chemometrics and Intelligent Laboratory Systems* (2009) **97** (2), 152

FIG.1

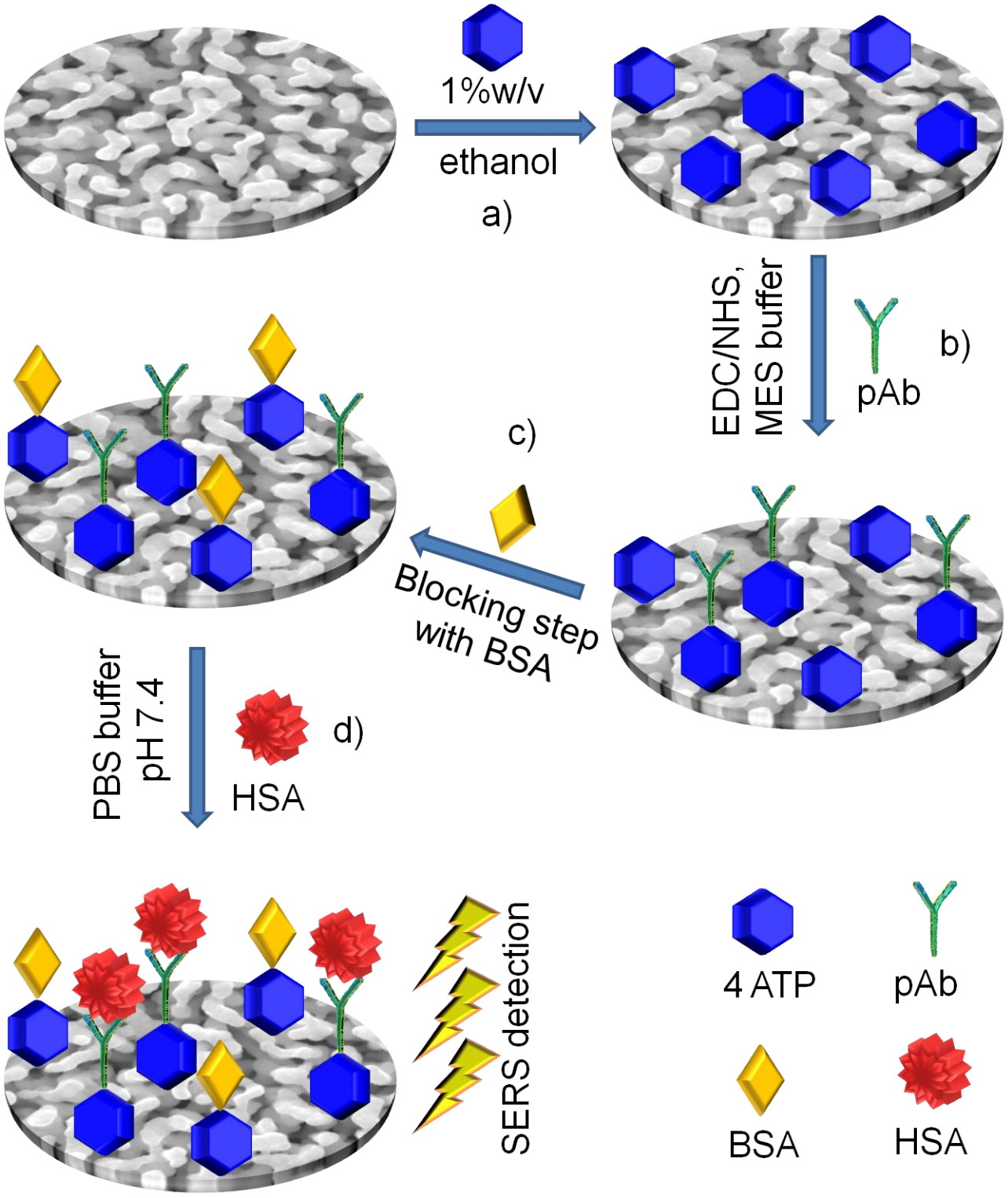

Figure 1. Step procedure for NPG functionalization **a)** cleaning and the synthesis of thiol derivative functionalized-NPG; **b)** covalent immobilization of pAb on 4-ATP NPG, **c)** A blocking step with BSA; **d)** Interaction of f-NPG with HSA.

FIG.2

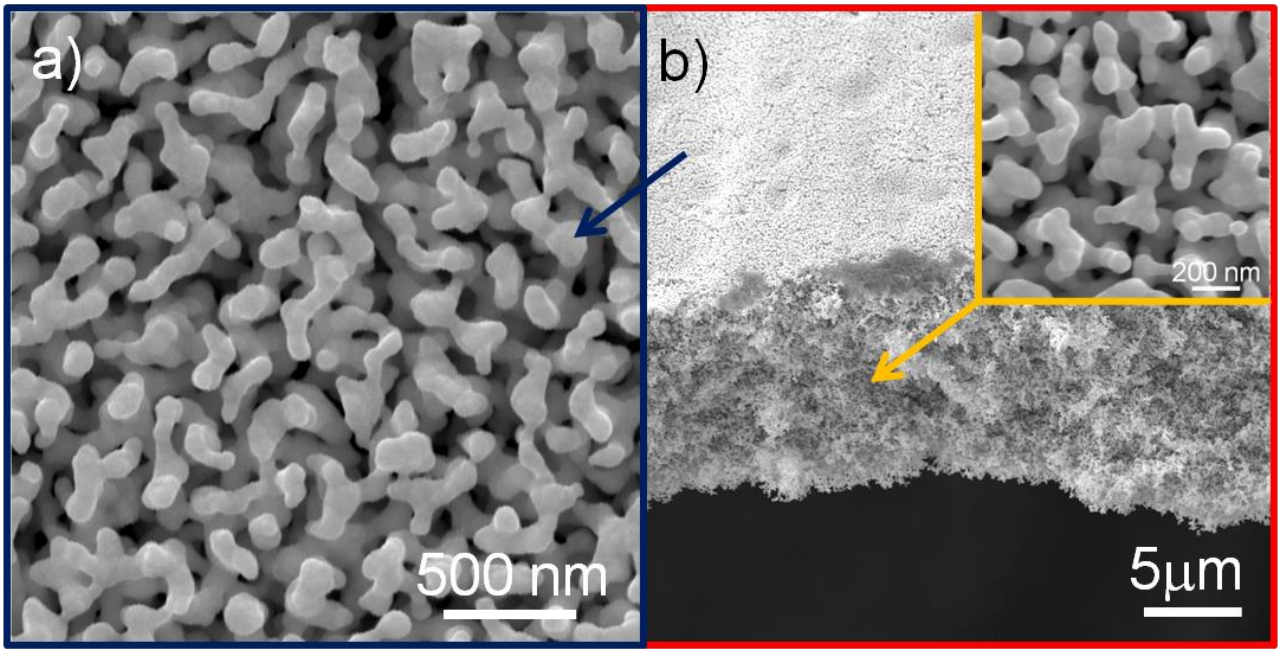

Figure 2. **a)** Top view SEM images of NPG after chemical de-alloying in 10 M HNO_3 + 0.5 M HF at 70 °C for 4 hours. **b)** Cross-section showing the fully de-alloying trough the thickness of the ribbon. In the inset, the nano-grained structure of ligaments in a magnification image inside the cross section.

FIG.3

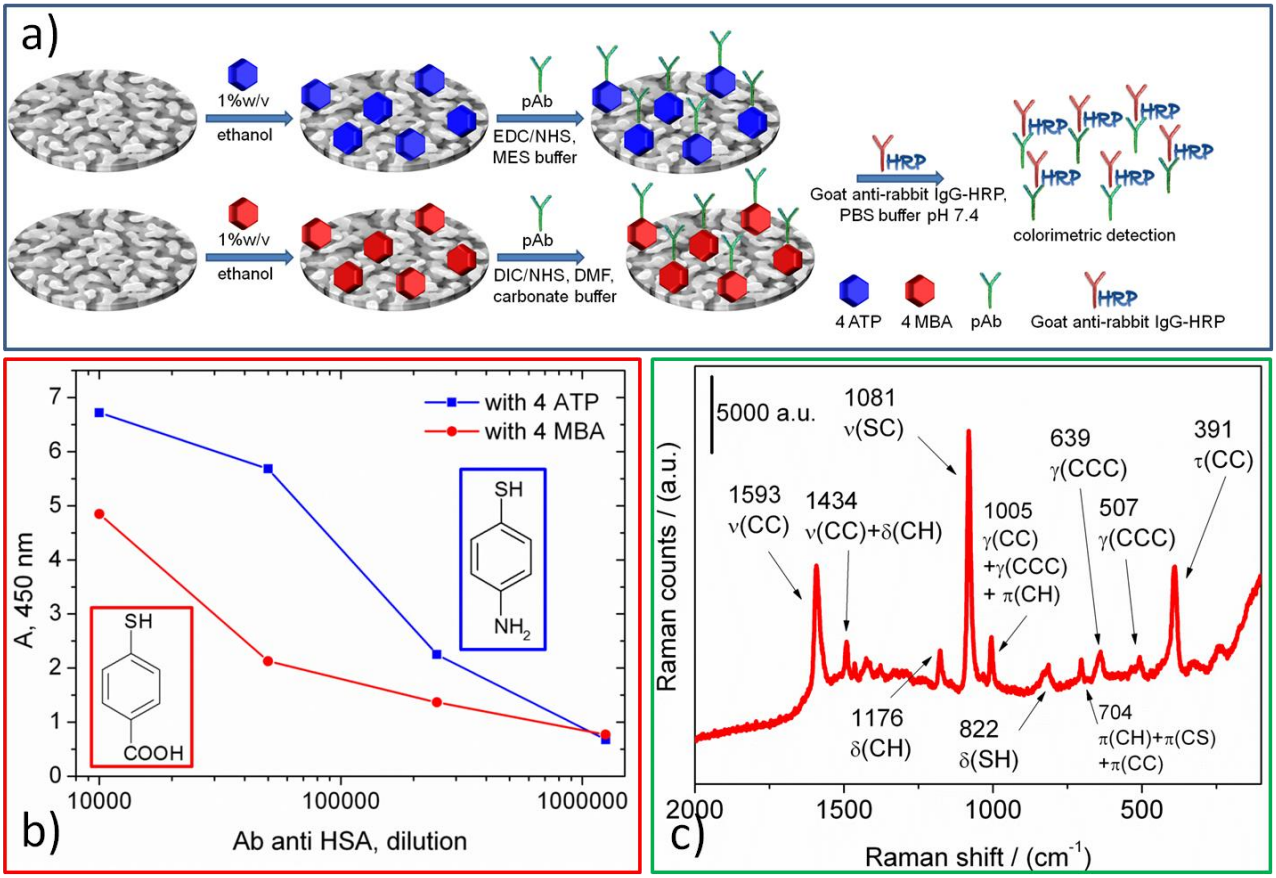

Figure. 3. a) Functionalization scheme of HRP-labelled anti-rabbit antibody bind to the anti-HSA antibody covalently immobilized on the surface. b) Colorimetric detection at 450 nm to determine the amount of anti-HSA antiserum covalently bonded to the surface functionalized with 4ATP or 4MBA. c) Full assignment of SERS signal of f-NPG. Peaks have been associated to vibrational mode of the 4ATP probe.

FIG.4

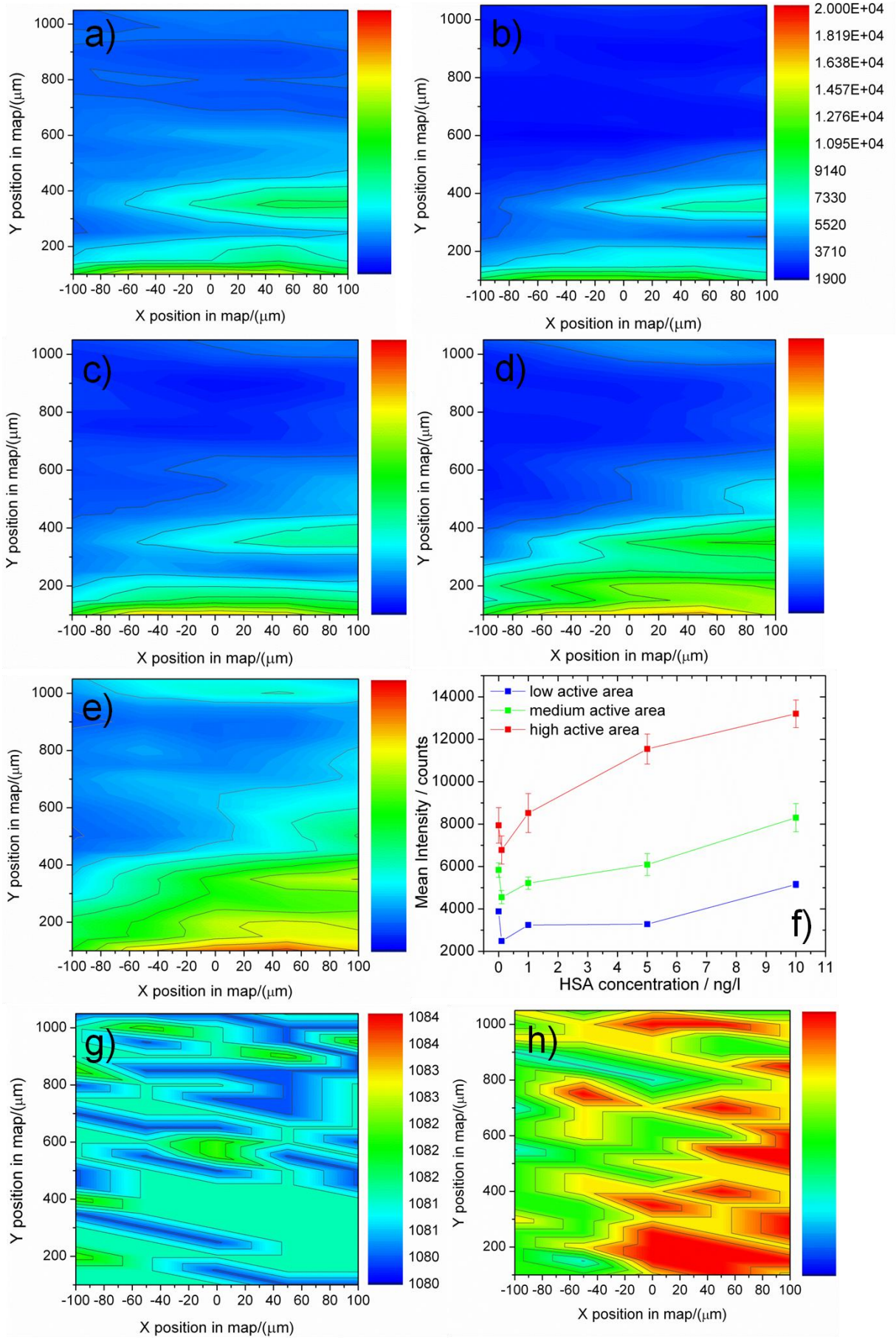
a)
b)
c)
d)
e)
f)
g)
h)
Y position in map/(μm)
X position in map/(μm)
2.000E+04
1.819E+04
1.638E+04
1.457E+04
1.276E+04
1.095E+04
9140
7330
5520
3710
1900
low active area
medium active area
high active area
Mean Intensity / counts
HSA concentration / ng/l
1084
1083
1082
1081
1080

Figure 4. ν(SC) peak intensity SERS maps of f-NPG after incubation with HSA solution at increasing concentration:
a) 0 ng/l, b) 0.1 ng/l, c) 1 ng/l, d) 5 ng/l, e) 10 ng/l. f) Mean Intensity vs HSA concentration dividing the maps points in three groups of colors. The error band is the standard error. ν(SC) peak shift SERS maps of f-NPG after incubation with HSA solution at increasing concentration: g) 0 ng/l, h) 10 ng/l. ν(SC) vibrational mode is shifted to higher values increasing HSA concentration.

FIG.5

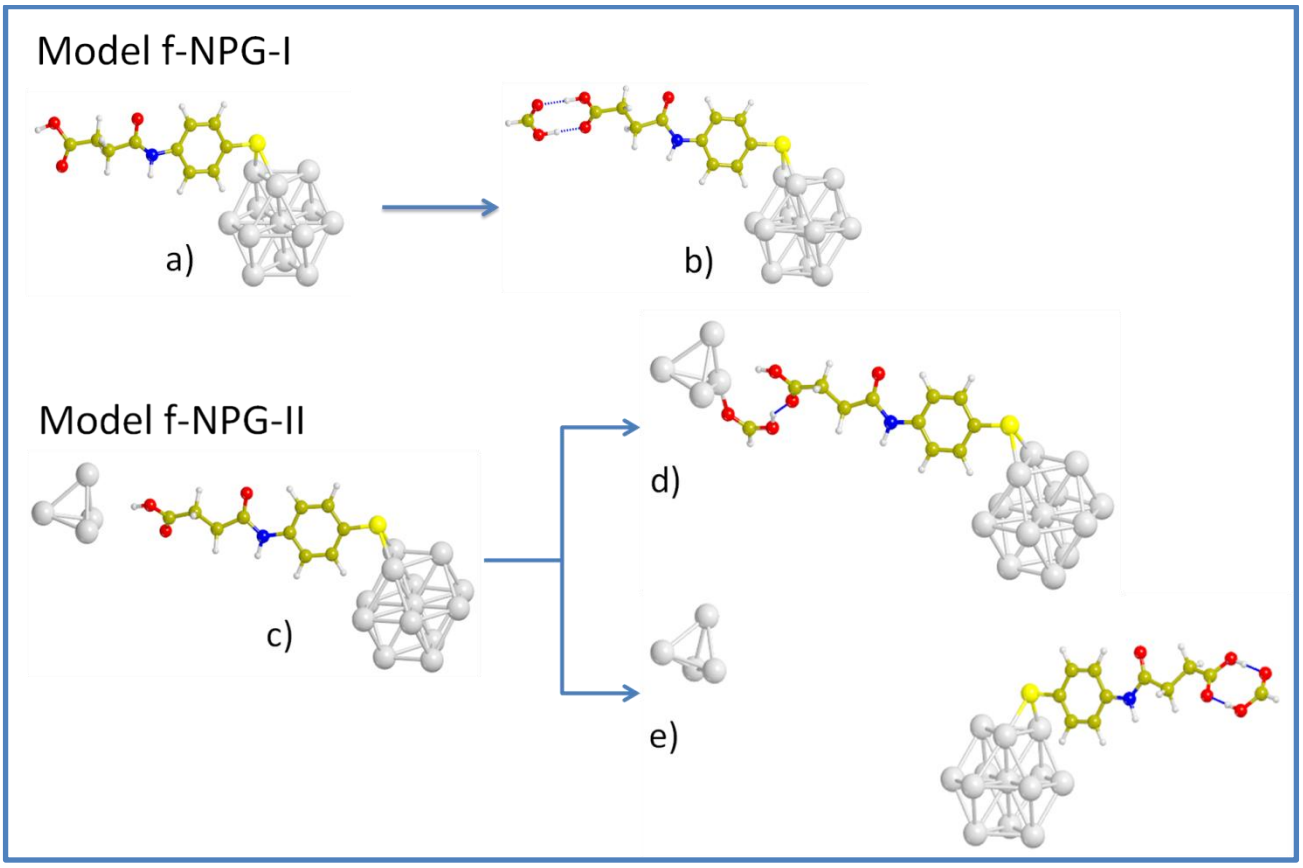

Figure 5. Simulated models of f-NPG-I, a) before target interaction (i.e. formic acid), b) after target interaction and of f-NPG-II with lateral interactions, c) before target interaction, d) and e) after target interaction in two possible configurations.

FIG.6

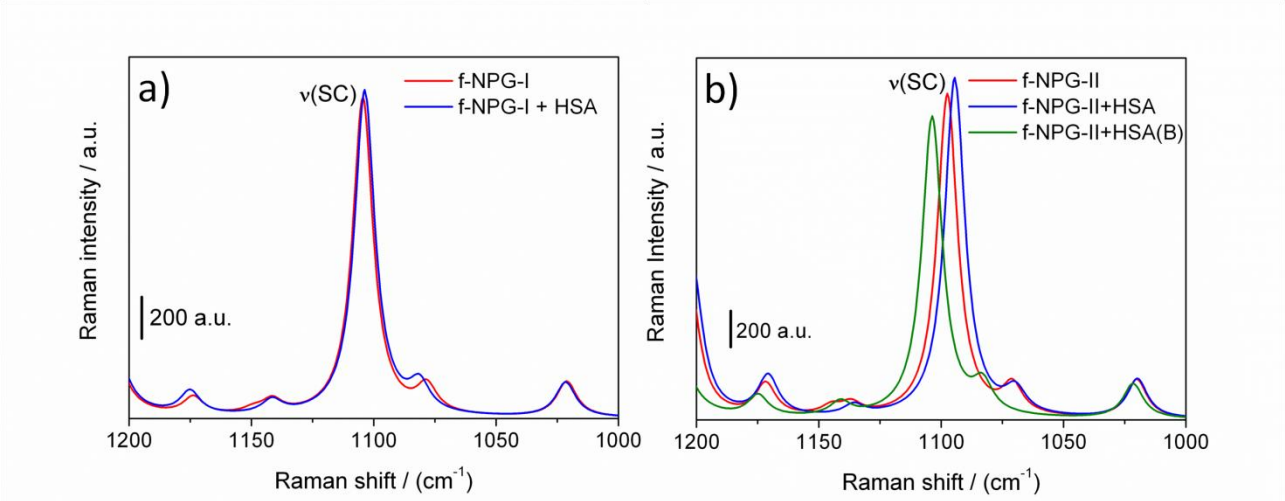

Figure 6. a) Computed Raman spectra of f-NPG-I before target interaction (red solid line) and after target interaction (blue solid line). b) Computed Raman spectra of f-NPG-II before target interaction (red solid line) and after target interaction; two configurations have been reported showing a red shift in one case (blue solid line) and a blue shift in the second case (B) (green solid line), this in agreement with experimental data.

FIG.7

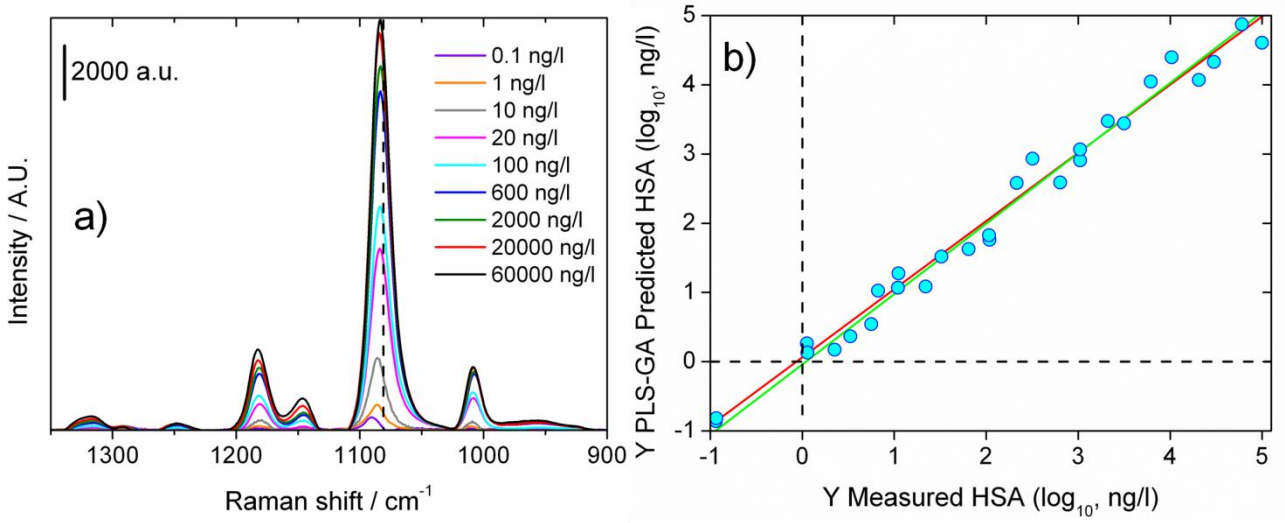

Figure 7. a) SERS spectra after the pre-processing techniques; the intensity of the ν(SC) peak increases as a function of HSA concentration. b) PLS-GA regression model - HSA measured vs HSA predicted plot. The x-axis represents the prepared and measured HSA concentrations (ng/l, log-10 scale), while the y-axis shows the HSA concentration levels estimated by the our model (ng/l, log-10 scale). The evaluated 28 samples are indicated by blue circles.

Highlights

1. Proof of concept of an ultra-sensitive biosensors for analytical devices with SERS
2. Nanoporous gold functionalized with a target-directed antibody (Ab anti-HSA)
3. Acquisition of detailed SERS maps at different HSA concentration
4. Chemometric approach to data analysis and sensor calibration
5. Biosensor gives quantitative analysis in ultra-low concentrations (0.1 ng/l)

Supplementary Material

Click here to download Supplementary Material: Sup. Info.docx